

# Electronic structure of helicoidal graphene: massless Dirac particles on a curved surface with a screw symmetry

Masataka Watanabe\*

*Department of Physics, The University of Tokyo, Hongo, Tokyo 133-0033, Japan*

Hisato Komatsu

*Department of Basic Science, The University of Tokyo, Komaba, Tokyo 153-8902, Japan*

Naoto Tsuji<sup>†</sup> and Hideo Aoki

*Department of Physics, The University of Tokyo, Hongo, Tokyo 133-0033, Japan*

Massless Dirac particles on the helicoid are theoretically investigated. With its possible application being helical graphene, we explore how the peculiarities of Dirac particles appear on the curved, screw-symmetric surface. Zweibein is used to derive the massless Dirac equation on the helicoid and on general curved surfaces. We show that bound states of massless Dirac electrons on the helicoid are shown to be absent, and thus the system is fully characterized by the scattering probabilities and the phase shifts. We obtained these quantities from numerically calculated wavefunctions. We find the local density of states and the phase shifts behave characteristically around the axis of the helicoid. Bound states of massive Dirac electrons on the surface are also shown to be absent as an extension of the above result on massless Dirac electrons. A comparison with the non-relativistic case is also made.

PACS numbers: 73.20.At, 02.40.-k

## I. INTRODUCTION

Graphene and massless Dirac fermions on it have gained persistent attention over the last few decades as a way of looking at relativity through condensed matter physics<sup>1</sup>. While there are a number of studies on graphene, only a few focus on curved graphene and its electronic structures. It is, therefore, worth asking the following question: how does the electronic structure of graphene change if we deform it into a curved surface? This is interesting in a number of ways. (i) Non-relativistic electrons on periodic curved surfaces have distinctive electronic structures<sup>2</sup> and we expect something even more interesting with Dirac fermions due to their spinor wavefunctions rather than scalar ones. (ii) It is also intriguing to see how the presence of positive and negative energy states of Dirac fermions exerts its effect on curved surfaces. In other words how the Klein paradox<sup>3</sup>, i.e., potential barriers cannot reflect massless Dirac particles, takes its form on curved surfaces.

These have motivated us to look into Dirac particles on the helicoid, one of the simplest curved surfaces periodic in one direction<sup>4</sup>. The surface is also simple in that it is a minimal surface, i.e., its mean curvature vanishes everywhere – it is the only ruled minimal surface other than the plane. Possible applications to physical systems include graphite with a screw dislocation. Horn for example reported a spiral growth patterns on natural graphite as early as 1952<sup>5</sup>, followed by more recent studies by Rakovan and Jaszczak<sup>6</sup>. There is also a theoretical study by Bird and Preston of a spiral graphite in terms of Berry's phase<sup>7</sup>.

The rest of the paper is organized as follows. In Section II we formulate the Dirac equation on general curved surfaces, and then in Section III apply the formalism to the helicoid. In Section III C we show that there are no bound states of

massless Dirac fermions on the helicoid and discuss the scattering amplitudes and the phase shifts of an electron off the spiral axis in terms of partial waves. We go on to discuss the local density of states in Section IV. In Section V we examine the (non-)existence of bound states of massive Dirac fermions on the helicoid. In Appendix B comparison with the non-relativistic case is briefly made.

## II. DIRAC EQUATION ON CURVED SURFACES

The massless Dirac equation on a flat two-dimensional surface,

$$i\sigma^\mu \partial_\mu \psi = E\psi, \quad (1)$$

describes the low-energy behaviour of electrons on graphene<sup>1</sup>. Here  $\sigma^\mu$  ( $\mu = 1, 2$ ) are the Pauli matrices,  $\psi$  is the spinor wavefunction, and  $E$  is the eigenenergy<sup>12</sup>. Here and hereafter repeated indices are implicitly summed over. We, following Birrell and Davies<sup>8</sup>, generalize the Dirac equation to curved surfaces by replacing derivatives with covariant derivatives,  $D_\mu$ , and by introducing zweibeins,  $e_a^\mu$ :

$$i\sigma^a e_a^\mu D_\mu \psi = E\psi \quad (a, \mu = 1, 2). \quad (2)$$

We take a convention in which the metric is given by  $g_{\mu\nu} = e_a^\mu e_b^\nu \eta_{ab}$  with  $\eta_{ab} = \text{diag}(+, -, -)$  being the Minkowskian metric. The covariant derivatives for spinors are given by  $D_\mu = \partial_\mu + \Gamma_\mu$ , where

$$\Gamma_\mu = \frac{1}{2} S^{ab} e_a^\nu g_{\rho\nu} D_\mu e_b^\rho \quad \text{and} \quad S^{ab} = \frac{1}{4} [\sigma^a, \sigma^b]. \quad (3)$$

The action of covariant derivatives on zweibeins is

$$D_\nu e_\mu^a = \partial_\nu e_\mu^a + e_\mu^b \omega_{b\nu}^a - e_\lambda^\lambda \Gamma_{\nu\mu}^\lambda. \quad (4)$$

Here  $\omega_{b\mu}^a$  are the spin connection coefficients defined via

$$d(e_\mu^a dx^\mu) = -\omega_b^a \wedge (e_\nu^b dx^\nu), \quad (5)$$

while  $\Gamma_{\nu\mu}^\lambda$  are the Christoffel symbols. We require the spin connection coefficients to be antisymmetric in  $a$  and  $b$  so as to avoid the arbitrariness in the above definition.

Every surface has global isothermal coordinates, i.e., every metric on any surfaces can be represented in a diagonal form upon a suitable coordinate transformation<sup>9</sup>:

$$g_{ij}(x, y) = \begin{pmatrix} g(x, y)^2 & 0 \\ 0 & g(x, y)^2 \end{pmatrix}. \quad (6)$$

The zweibeins and Christoffel symbols then read, in matrix forms,

$$\begin{aligned} e_\mu^a &= \begin{pmatrix} g(x, y) & 0 \\ 0 & g(x, y) \end{pmatrix}, \quad e_a^\mu = \begin{pmatrix} g(x, y)^{-1} & 0 \\ 0 & g(x, y)^{-1} \end{pmatrix}, \\ \Gamma_{\kappa 1}^\rho &= \frac{1}{2} \begin{pmatrix} g^{-2} \partial_1(g^2) & g^{-2} \partial_2(g^2) \\ g^{-2} \partial_2(g^2) & -g^{-2} \partial_1(g^2) \end{pmatrix}, \\ \Gamma_{\kappa 2}^\rho &= \frac{1}{2} \begin{pmatrix} g^{-2} \partial_2(g^2) & -g^{-2} \partial_1(g^2) \\ g^{-2} \partial_1(g^2) & g^{-2} \partial_2(g^2) \end{pmatrix}. \end{aligned} \quad (7)$$

The spin connections are calculated as

$$\begin{cases} \omega_{21}^1 = \frac{1}{g} \partial_2(g), \\ \omega_{12}^2 = \frac{1}{g} \partial_1(g), \\ \omega_{\mu b}^a = 0. \end{cases} \quad (\text{other components}) \quad (8)$$

By substituting these into Eq. (2), we arrive at the massless Dirac equation on a curved surface in terms of isothermal coordinates:

$$i \begin{pmatrix} 0 & \frac{1}{g} \partial \\ \frac{1}{g} \bar{\partial} & 0 \end{pmatrix} \begin{pmatrix} \sqrt{g} \psi_+ \\ \sqrt{g} \psi_- \end{pmatrix} = E \begin{pmatrix} \sqrt{g} \psi_+ \\ \sqrt{g} \psi_- \end{pmatrix}, \quad (9)$$

where  $\partial \equiv \partial_x - i\partial_y$ ,  $\bar{\partial} \equiv \partial_x + i\partial_y$  and  $\psi_+$ ,  $\psi_-$  are two components of the spinor<sup>13</sup>. It is easy to see that Eq. (9) has a chiral symmetry<sup>1</sup> since the equation has a solution with eigenenergy  $-E$  accompanied with a solution with eigenenergy  $E$ :

$$i \begin{pmatrix} 0 & \frac{1}{g} \partial \\ \frac{1}{g} \bar{\partial} & 0 \end{pmatrix} \begin{pmatrix} \sqrt{g} \psi_+ \\ -\sqrt{g} \psi_- \end{pmatrix} = -E \begin{pmatrix} \sqrt{g} \psi_+ \\ -\sqrt{g} \psi_- \end{pmatrix}. \quad (10)$$

Moreover, the system has a zero-mode, where  $\sqrt{g} \psi_+$  and  $\sqrt{g} \psi_-$  are holomorphic and anti-holomorphic, respectively.

### III. DIRAC EQUATION ON THE HELICOID

The helicoid, shown in Fig. 1, can be parametrized in  $\mathbb{R}^3 \ni (x, y, z)$  as

$$\begin{pmatrix} x \\ y \\ z \end{pmatrix} = a \begin{pmatrix} \sinh u \cos v \\ \sinh u \sin v \\ v \end{pmatrix}, \quad (11)$$

where the coordinate  $v$  spirals about the axis of the helicoid, while  $u$  shoots out normal to  $v$  from the axis with  $a$  being the pitch of the spiral. The metric in this parametrization is

$$g_{ij} = \begin{pmatrix} a \cosh^2 u & 0 \\ 0 & a \cosh^2 u \end{pmatrix}, \quad (12)$$

which indicates that  $(u, v)$  are indeed isothermal.

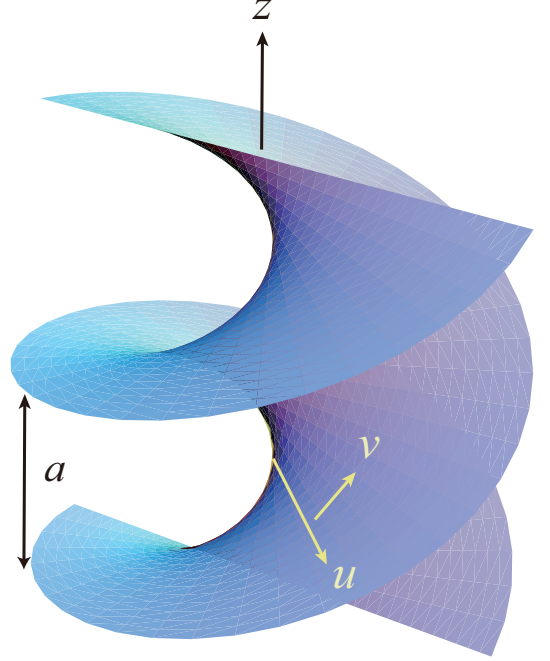


FIG. 1: (Color online) A helicoid in three-dimensional Euclidean space. Shown on the surface are the isothermal coordinates,  $(u, v)$ .

The massless Dirac equation (9) on the helicoid then reads

$$\frac{i}{a \cosh u} \begin{pmatrix} 0 & \partial_u - i\partial_v + \frac{\tanh u}{2} \\ \partial_u + i\partial_v + \frac{\tanh u}{2} & 0 \end{pmatrix} \begin{pmatrix} \psi_+ \\ \psi_- \end{pmatrix} = E \begin{pmatrix} \psi_+ \\ \psi_- \end{pmatrix}. \quad (13)$$

Since  $v$  is a cyclic coordinate, representing the translational symmetry along the axis of the helicoid, we can set

$$\psi_\pm(u, v) = \exp(i\ell v) \phi(u)_\pm, \quad (14)$$

in which  $\ell$  is physically the “angular momentum” along the  $z$  axis. Since the system is helical and the coordinate  $v$  spirals around the axis of the helicoid,  $\ell$  does not necessarily have to be integer-valued, or cannot be quantized. This angular momentum,  $\ell$ , can also be regarded as the momentum along the helical axis. This leaves us with a differential equation for  $\phi(u)$  below:

$$\frac{i}{\cosh u} \begin{pmatrix} 0 & \partial_u + \ell + \frac{\tanh u}{2} \\ \partial_u - \ell + \frac{\tanh u}{2} & 0 \end{pmatrix} \begin{pmatrix} \phi_+ \\ \phi_- \end{pmatrix} = E \begin{pmatrix} \phi_+ \\ \phi_- \end{pmatrix}. \quad (15)$$

We took a unit in which  $a = 1$  here. We are going to stick with this unit system unless otherwise stated.

### A. Solving the Equation with fixed $\ell$

The massless Dirac equation on the helicoid, (15), is similar to the flat-space Dirac equation in that it takes an off-diagonal form,

$$\begin{pmatrix} 0 & \frac{iD_\ell}{\cosh u} \\ \frac{iD_{-\ell}}{\cosh u} & 0 \end{pmatrix} \begin{pmatrix} \phi_+ \\ \phi_- \end{pmatrix} = E \begin{pmatrix} \phi_+ \\ \phi_- \end{pmatrix}, \quad (16)$$

where

$$D_\ell = \partial_u + \ell + \frac{\tanh u}{2}. \quad (17)$$

We square the Dirac Hamiltonian,  $\begin{pmatrix} 0 & \frac{iD_\ell}{\cosh u} \\ \frac{iD_{-\ell}}{\cosh u} & 0 \end{pmatrix}$ , to get a set of second-order differential equations:

$$\frac{1}{\cosh u} D_\ell \frac{1}{\cosh u} D_{-\ell} \phi_+ = E^2 \phi_+ \quad (18)$$

$$\frac{1}{\cosh u} D_{-\ell} \frac{1}{\cosh u} D_\ell \phi_- = E^2 \phi_-. \quad (19)$$

Although it is possible to numerically solve these equations directly, one alternative is to cast them into a more convenient, Schrödinger-type form with the transformations below:

$$s = \sinh(u) \quad \text{and} \quad \psi_\pm(u) = \phi_\pm(u) \sqrt{\cosh u}. \quad (20)$$

This transformation is chosen for geometric reasons: (i)  $ds$  gives the infinitesimal canonical distance in  $\mathbb{R}^3$ . (ii) The integral measure,  $\cosh u du$ , associated with the metric, Eq. (12), is then factored out. Following these, Eq. (19) is transformed into

$$-\frac{d^2}{ds^2} \psi(s) + \left[ \frac{\ell^2}{1+s^2} - \frac{\ell s}{(1+s^2)^{3/2}} \right] \psi(s) = E^2 \psi(s). \quad (21)$$

We concentrate only on the  $\psi_-(s) \equiv \psi(s)$  component of the spinor here and hereafter: we only have to change  $\ell$  into  $-\ell$  to obtain the  $\psi_+(s)$  component of the spinor. Eq. (21), is just the one-dimensional Schrödinger equation with eigenenergy  $E^2$  for a particle with mass  $m = 1/2$  travelling through the potential barrier

$$V_\ell(s) = \frac{\ell^2}{1+s^2} - \frac{\ell s}{(1+s^2)^{3/2}} \quad (22)$$

(see Fig. 2). Note that  $E^2$  on the right-hand side of Eq. (21) ensures we can concentrate only on non-negative eigenvalues of this eigenvalue equation.

The potential barrier,  $V_\ell(s)$ , approaches zero as  $s \rightarrow \pm\infty$  (Fig. 2). This implies we have no bound states with energy above zero. Therefore all the states we need to consider (with eigenenergy  $E^2$  nonnegative) are scattering states, and we have to solve the equation with boundary conditions in which eigenstates behave asymptotically like plane waves as  $s \rightarrow \pm\infty$ . Examples of numerically obtained wavefunctions are shown in Fig. 3, along with their asymptotes. We have employed the Runge-Kutta method and solved the differential equation backwards from  $s_0 = 45$ , with its initial

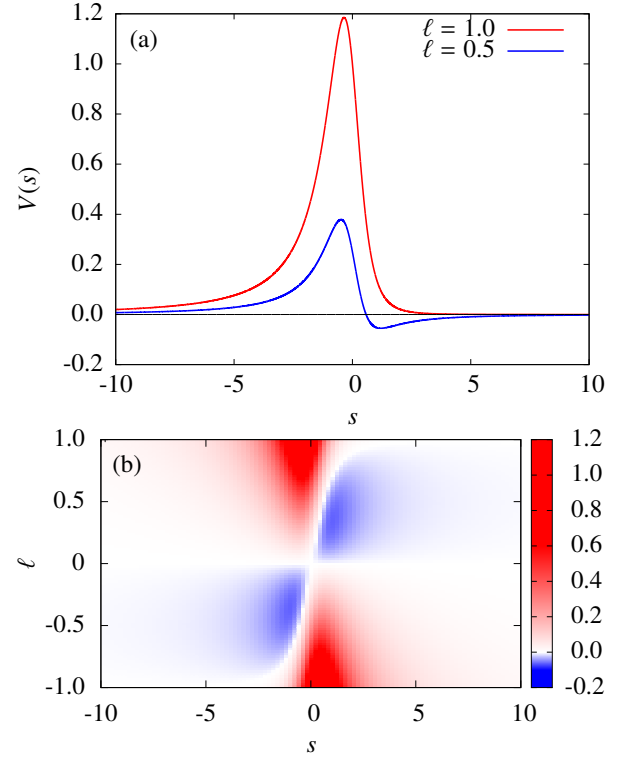


FIG. 2: (Color online) (a) The potential barrier in the transformed one-dimensional problem as functions of  $s = \sinh(u)$  with different values of  $\ell$ . (b) 2D color map of the potential against  $\ell$  and  $s$ .

value conditions chosen to match the real/imaginary parts of  $\psi(s_0) = \exp(iEs_0)$  and  $\psi'(s_0) = iE \exp(iEs_0)$ . We can see from the figure that the wavefunctions deviate from the asymptotic plane waves in a region very close to the axis of the helicoid ( $s \sim 0$ ).

We then calculate the reflection and transmission coefficients,  $\mathcal{R} \equiv Re^{i\delta_R}$  and  $\mathcal{T} \equiv Te^{i\delta_T}$ , using the obtained wavefunctions and their asymptotes (see Fig. 4). The results are plotted against  $E$  in Fig. 5.

We can see from the figure that the transmission/reflection probabilities resemble those of a finite potential barrier, except that the resonance phenomena does not show up in the present system. This is because the potential barrier  $V_\ell(s)$  is somewhat rounded compared with finite hard walls. The wavelength of electrons are much shorter than the typical scale at which the height of the potential changes.

### B. Solving the Equation with fixed $E$

We also plot  $R$  and  $T$  against  $\ell$  (Fig. 6). We can see from Fig. 6 that  $|T|^2$ ,  $|R|^2$  and  $\arg T$  are invariant while  $\arg R$  increases by  $\pi$  under the inversion of the angular momentum ( $\ell \mapsto -\ell$ ). The reason why there is such a symmetry will be discussed in the next section.

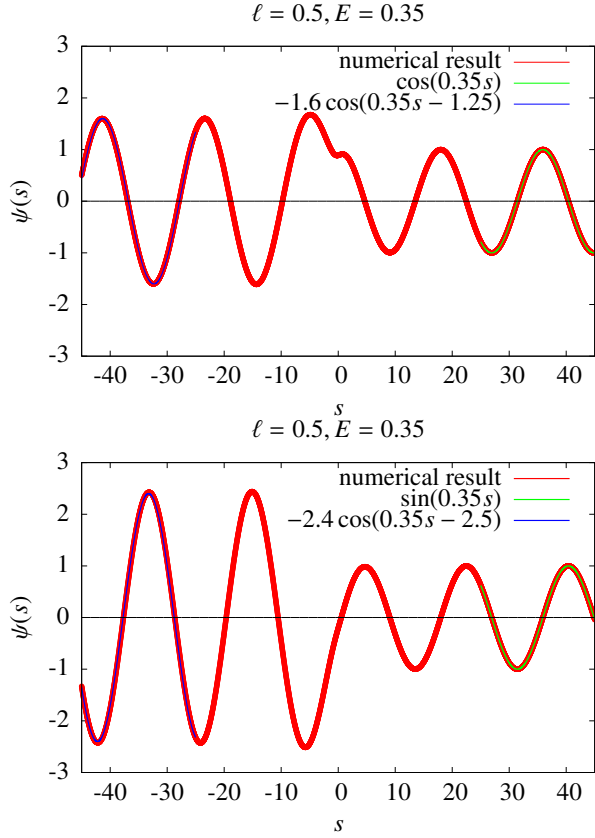


FIG. 3: (Color online) The wavefunction with  $\ell = 0.5$  at  $E = 0.35$  (the red, thick curves). The green, thin curves on the right side ( $25 < s < 50$ ) represent positive asymptotes, i.e.,  $\cos(Es)$  and  $\sin(Es)$  in the upper and lower panel, respectively. The blue, thin curves on the left side ( $-50 < s < -25$ ) are fitted curves representing negative asymptotes.

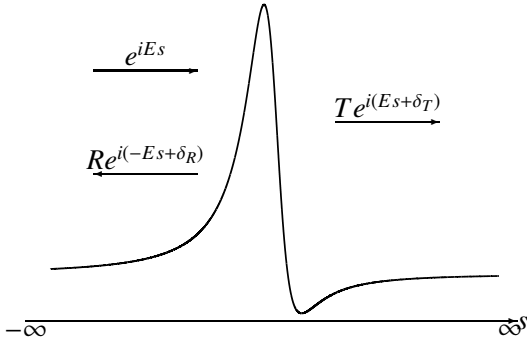


FIG. 4: The boundary condition of the system as a transformed one-dimensional problem.

### C. Scattering amplitudes and phase shifts against $\ell$ and $E$

Let us summarize the above results into two-dimensional plots against  $\ell$  and  $E$  of  $|\mathcal{T}|^2$ ,  $|\mathcal{R}|^2$ ,  $\arg \mathcal{T}$ , and  $\arg \mathcal{R}$ . These are shown in Fig. 7.

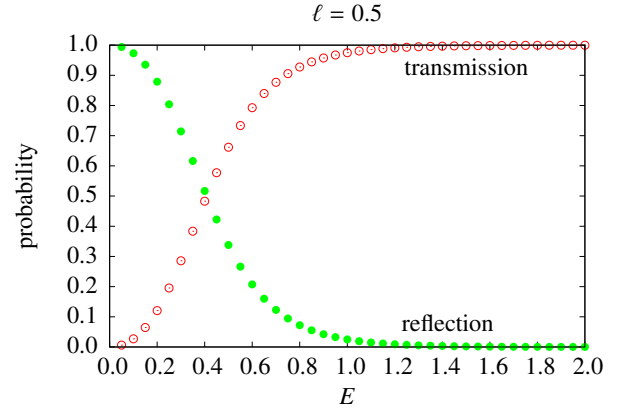


FIG. 5: (Color online) The transmission/reflection probabilities with  $\ell = 0.5$  plotted against energy.

Physical quantities tend to change significantly where the eigenenergy  $E^2$  becomes comparable with the peak height of the potential:

$$E^2 \sim \frac{2}{27} \left[ |\ell|(\ell^2 + 3)^{3/2} - \ell^2(\ell^2 - 9) \right] \sim \ell^2 \quad (\ell \gtrsim O(1)). \quad (23)$$

This corresponds to the line where physical quantities change considerably in Fig. 7 (the green regions in (a), the purple and aqua regions in (b) and the purple regions in (c)).

One interesting question worth asking here is how the transmission/reflection coefficients associated with some positive angular momentum  $\ell$  (i.e., electrons spiralling upwards in the  $+z$  direction) are related to those associated with the inverted angular momentum,  $-\ell$  (electrons spiralling downwards in the  $-z$  direction). In the transformed one-dimensional problem, the relation  $V_\ell(s) = V_{-\ell}(-s)$  implies the following: inverting the angular momentum ( $\ell \mapsto -\ell$ ) amounts to inverting  $s$  with  $\ell$  fixed ( $s \mapsto -s$ ). We are, therefore, going to discuss the change in physical quantities in terms of the space inversion.

We define the transfer matrix as described in Fig. 8:

$$\begin{pmatrix} A \\ B \end{pmatrix} = \hat{T} \begin{pmatrix} C \\ D \end{pmatrix}, \quad \hat{T} = \begin{pmatrix} p & r \\ q & s \end{pmatrix}. \quad (24)$$

The relations between the variables above and those in Fig. 4 are  $1/p = \mathcal{R} \equiv R e^{i\delta_R}$  and  $q/p = \mathcal{T} \equiv T e^{i\delta_T}$ . The probability conservation requires  $|p|^2 - |q|^2 = 1$  as well as the existence of  $\Delta$  such that  $r = q^* e^{i\Delta}$  and  $s = p^* e^{i\Delta}$  hold<sup>14</sup>.

The space-inverted transfer matrix  $\hat{T}'$  satisfies, by definition, the following:

$$\begin{pmatrix} D \\ C \end{pmatrix} = \hat{T}' \begin{pmatrix} B \\ A \end{pmatrix}, \quad \hat{T}' = \begin{pmatrix} p e^{-i\Delta} & -q e^{-i\Delta} \\ -q^* & p^* \end{pmatrix}. \quad (25)$$

This means that the transmission/reflection coefficients,  $\mathcal{T}$  and  $\mathcal{R}$ , of the inverted system are  $e^{i\Delta}/p$  and  $-(q^*/p)e^{i\Delta}$ , respectively. The transmission/reflection probabilities,  $|\mathcal{T}|^2$  and  $|\mathcal{R}|^2$ , are therefore invariant under the space inversion. We can also show

$$\Delta \approx 0, \quad \arg q \propto \frac{1}{E} \rightarrow 0 \quad (E \rightarrow \infty) \quad (26)$$

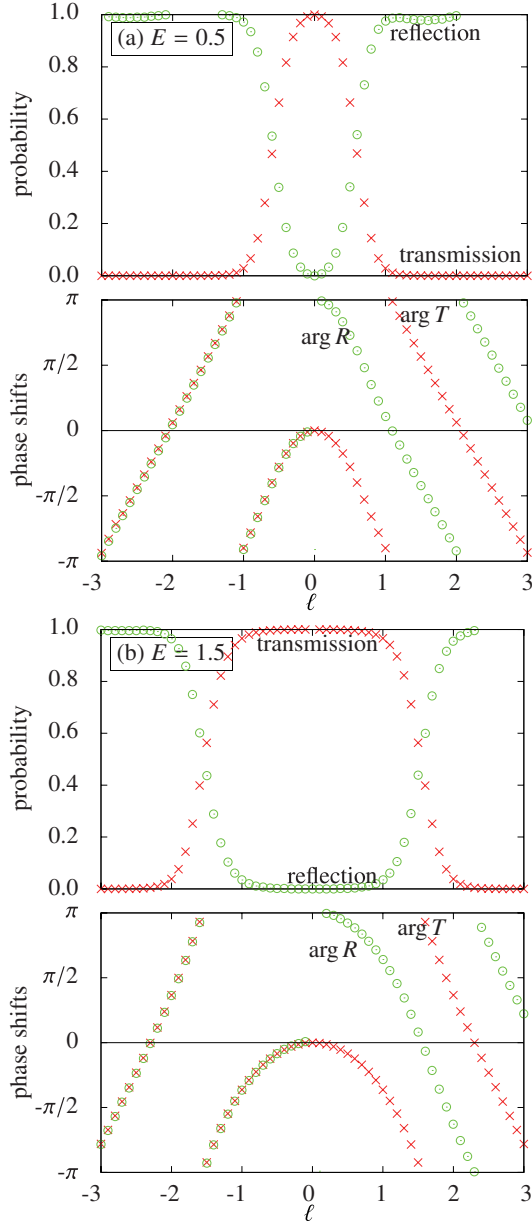


FIG. 6: (Color online) The transmission and the reflection probabilities and the phase shifts plotted against  $\ell$  at (a)  $E = 0.5$  and (b)  $E = 1.5$ .

using the first Born approximation. This is shown in Appendix A. This relation holds to a good approximation, according to our numerical calculation. This is the reason why, as we can see in Fig. 6, the phase shift of the transmitted wave is symmetric about  $\ell = 0$  while that of the reflected wave is symmetric otherwise a jump by  $\pi$  at  $\ell = 0$ .

It might first seem strange that inverting angular momentum should bring about changes in any physical quantities. However, as we are dealing with spinors here<sup>15</sup>, only when the angular momentum and the spin directions are both inverted will the system go back to its original state. This operation corresponds to inverting  $\ell$  and  $s$  simultaneously.

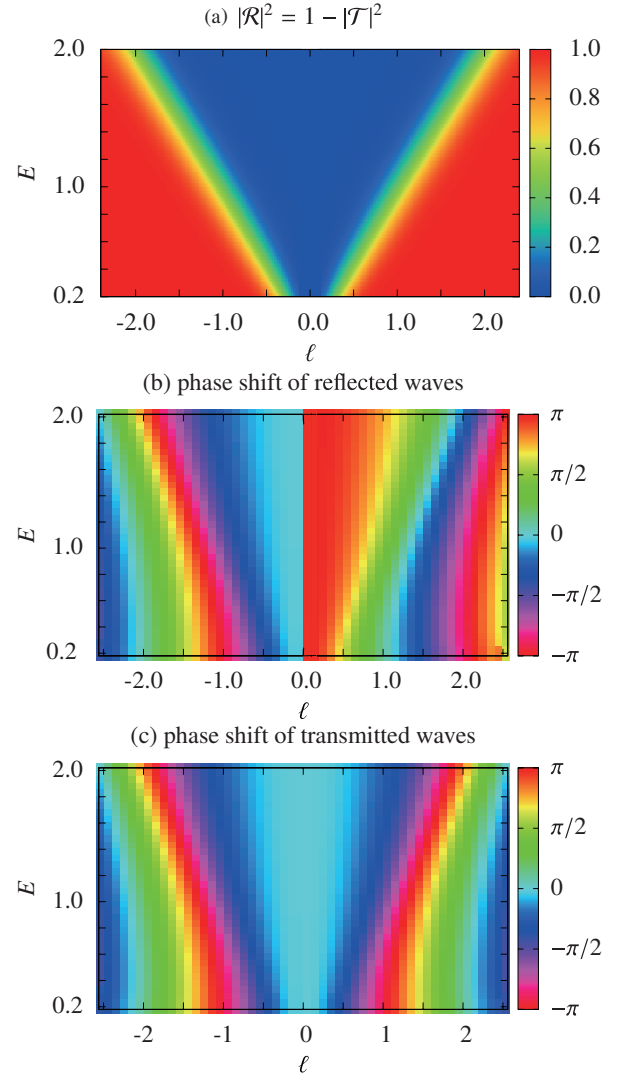


FIG. 7: (Color online) (a) 2D colour map of the reflection probability ( $|R|^2 = 1 - |T|^2$ ) on  $\ell$  and  $E$ . (b) 2D colour map of the reflection phase shifts on  $\ell$  and  $E$ . (c) 2D colour map of the transmission phase shifts on  $\ell$  and  $E$ .

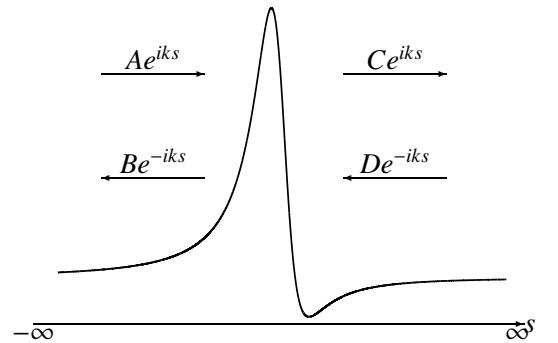


FIG. 8: Incoming and outgoing waves.

#### IV. LOCAL DENSITY OF STATES

We now turn to the local density of states (LDoS) of the system. This is one way of visualising wavefunctions when dealing with continuous spectra. LDoS,  $\rho(\mathbf{r}, E)$ , is defined, in terms of the Green's function, as

$$\rho(\mathbf{r}, E) = \frac{1}{\pi} \text{Im Tr } G(\mathbf{r}, \mathbf{r}, E). \quad (27)$$

where  $G(\mathbf{r}, \mathbf{r}', E)$  is the Green's function and is a  $2 \times 2$  matrix:

$$G(\mathbf{r}, \mathbf{r}', E) = \begin{pmatrix} G^{++}(\mathbf{r}, \mathbf{r}', E) & G^{+-}(\mathbf{r}, \mathbf{r}', E) \\ G^{-+}(\mathbf{r}, \mathbf{r}', E) & G^{--}(\mathbf{r}, \mathbf{r}', E) \end{pmatrix}. \quad (28)$$

The Green's function for the Dirac equation

$$\begin{pmatrix} 0 & D^+ \\ D^- & 0 \end{pmatrix} \begin{pmatrix} \psi_n^+ \\ \psi_n^- \end{pmatrix} = E_n \begin{pmatrix} \psi_n^+ \\ \psi_n^- \end{pmatrix}, \quad (29)$$

satisfies the following relation :

$$\left[ \begin{pmatrix} 0 & D^+(\mathbf{r}) \\ D^-(\mathbf{r}) & 0 \end{pmatrix} - E \right] \begin{pmatrix} G^{++}(\mathbf{r}, \mathbf{r}', E) & G^{+-}(\mathbf{r}, \mathbf{r}', E) \\ G^{-+}(\mathbf{r}, \mathbf{r}', E) & G^{--}(\mathbf{r}, \mathbf{r}', E) \end{pmatrix} = -\delta(\mathbf{r} - \mathbf{r}') \mathbf{1}, \quad (30)$$

This gives a spectral representation of the Green's function:

$$G^{++}(\mathbf{r}, \mathbf{r}', E) = -\lim_{\delta \rightarrow 0} \sum_n \frac{E \psi_n^+(\mathbf{r}') \psi_n^+(\mathbf{r})}{E^2 - E_n^2 + i\delta}, \quad (31)$$

$$G^{--}(\mathbf{r}, \mathbf{r}', E) = -\lim_{\delta \rightarrow 0} \sum_n \frac{E \psi_n^-(\mathbf{r}') \psi_n^-(\mathbf{r})}{E^2 - E_n^2 + i\delta}, \quad (32)$$

where we have assumed the completeness of  $\{\psi_n^+(\mathbf{r})\}$  and of  $\{\psi_n^-(\mathbf{r})\}$ , respectively. LDoS is then given by

$$\rho(\mathbf{r}, E) = \sum_n E \delta(E^2 - E_n^2) [|\psi_n^+(\mathbf{r})|^2 + |\psi_n^-(\mathbf{r})|^2], \quad (33)$$

or

$$\rho(\mathbf{r}, E) = \frac{1}{2} \sum_{\alpha=\pm} [|\psi_E^{\alpha,1}(\mathbf{r})|^2 + |\psi_E^{\alpha,2}(\mathbf{r})|^2], \quad (34)$$

if we have a continuous spectrum. Here we let  $\{\psi_E^{\pm,1}(\mathbf{r}), \psi_E^{\pm,2}(\mathbf{r})\}$  form an orthonormal basis of the eigenspace of  $D^\pm(\mathbf{r})D^\mp(\mathbf{r})$  with eigenvalue  $E^2$ .

We can Fourier transform Green's function on the helicoid with respect to  $v$  to decompose LDoS into partial LDoS,  $\rho_\ell(s, E)$ :

$$\rho(s, E) = \sum_\ell \rho_\ell(s, E) = \sum_\ell \sum_{\alpha=\pm} [|\psi_{\ell,E}^{\alpha,1}(s)|^2 + |\psi_{\ell,E}^{\alpha,2}(s)|^2]. \quad (35)$$

We calculate partial LDoS numerically. As the original wavefunctions (asymptotically  $\cos(ks)$  and  $\sin(ks)$  as  $s \rightarrow \infty$ ) do not form an orthonormal basis, we have to prepare  $\psi_E^{\pm,1}(s)$  and  $\psi_E^{\pm,2}(s)$  which are orthogonal and normalised. This orthogonalization of the actual wavefunctions was done using the Gram-Schmidt algorithm. The numerically calculated

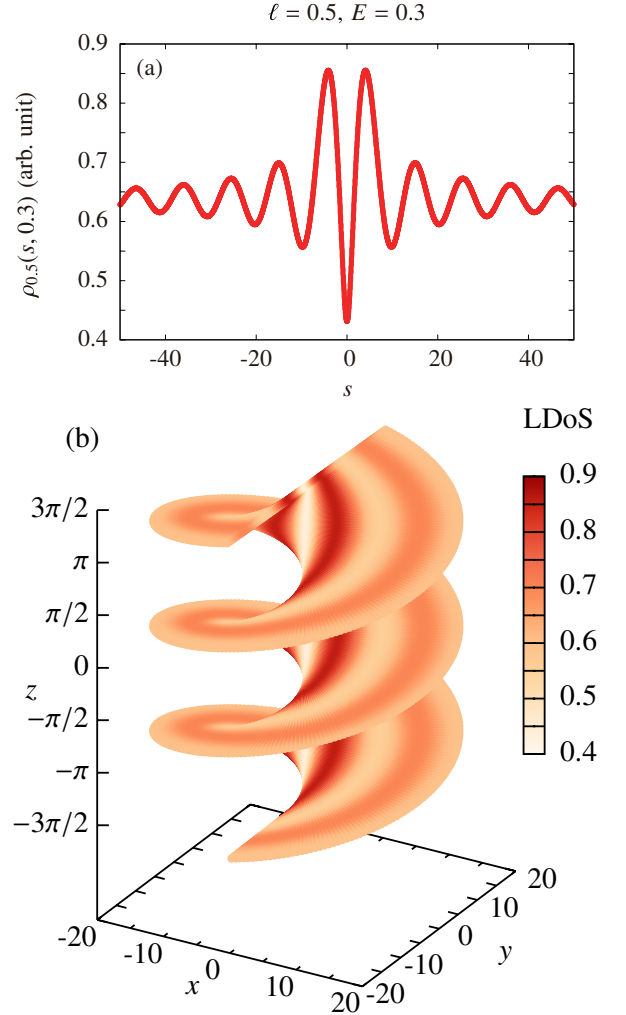


FIG. 9: (Color online) (a) Local density of states on the helicoid on  $s$  with  $\ell = 0.5$  at  $E = 0.3$ . Note the symmetry with respect to the space inversion,  $s \mapsto -s$ . (b) Surface color plot of LDoS on the helicoid.

LDoS is shown in Fig. 9. We can see that LDoS oscillates with large amplitudes in the vicinity of the axis of the helicoid. This is natural because the potential is peaked around  $s = \sinh(u) \approx 0$  (see Fig. 2). We also plot LDoS against  $E$  and  $s$  or against  $\ell$  and  $s$ . These are shown in Fig. 10. Again LDoS oscillates with large amplitudes around the axis of the helicoid in a consistent way: faster oscillations for larger  $E$ , and smaller amplitudes for larger  $\ell$ .

#### V. MASSIVE CASE

Having studied the case of massless Dirac fermions so far, let us move on to the case of massive Dirac fermions on the helicoid. One might expect that bound states could appear in the massive case, for which we replace  $E^2$  with  $E^2 - m^2$  in Eq.



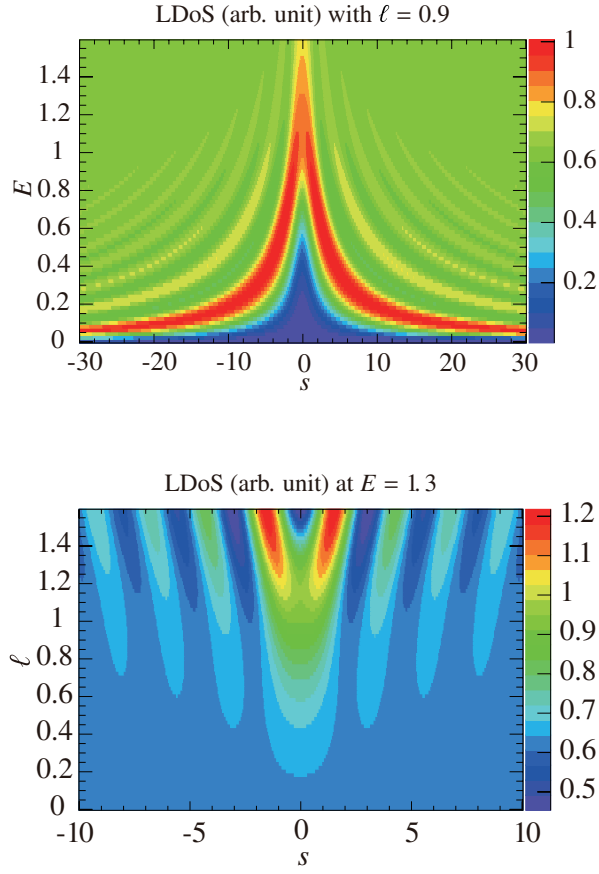


FIG. 10: (Color online) Local density of states against  $E$  and  $s$  (upper) or against  $\ell$  and  $s$  (lower).

(21):

$$-\frac{d^2}{ds^2}\psi(s) + \left[ \frac{\ell^2}{1+s^2} - \frac{\ell s}{(1+s^2)^{3/2}} \right] \psi(s) = (E^2 - m^2)\psi(s). \quad (36)$$

We can however prove that bound states continue to be absent even in the massive case.

In order to show the absence of bound states with  $E^2 - m^2 < 0$ , we only have to find one wavefunction whose eigenenergy satisfies  $E^2 - m^2 = 0$  that is everywhere nodeless. This can most easily be done by going back to the original Dirac equation, (15). At  $E = 0$ , this equation becomes, for  $\phi_-$ ,

$$\left[ \frac{d}{du} + \ell + \frac{\tanh(u)}{2} \right] \phi_- = 0, \quad (37)$$

which can be solved analytically to give

$$\phi_-(u) = \frac{e^{-\ell u}}{\sqrt{\cosh u}}. \quad (38)$$

This can be translated into a wavefunction of the Schrödinger-type equation, (36), with its eigenenergy satisfying  $E^2 - m^2 = 0$ :

$$\psi_-(s) = \phi_-(u) \sqrt{\cosh u} = e^{-\ell u} > 0, \quad (39)$$

where  $s = \sinh u$  as before<sup>16</sup>. This means that one of the wavefunctions of the states with  $E^2 - m^2 = 0$  is nodeless (hence a ground state wavefunction), which means there are no bound states at  $E^2 - m^2 < 0$ . We therefore conclude the absence of bound states even in the case of massive Dirac particles.

We can also show that the state with  $E^2 - m^2 = 0$  is actually the ground state on any surfaces if they have at least one cyclic coordinate. According to Eq. (9), the zero-energy wavefunctions satisfy the following differential equation:

$$(\partial_x - \partial_y) \left[ \sqrt{g(x,y)} \psi_-(x,y) \right] = 0 \quad (40)$$

(see Eqs. (6, 9) for how  $g$  and  $\psi_-$  are defined). We think of  $y$  as the cyclic coordinate conjugate to the momentum  $k$ , and the above equation becomes

$$(\partial_x + k) \left[ \sqrt{g(x)} \phi_-(x) \right] = 0, \quad (41)$$

which again can be solved analytically to give

$$\phi_-(x) = \frac{e^{-kx}}{\sqrt{g(x)}}. \quad (42)$$

In the Schrödinger-type notation the wavefunction is

$$\psi(x) = \phi_-(x) \sqrt{g(x)} = e^{-kx} > 0 \quad (43)$$

in agreement with Eq. (39) in the case of the helicoid. Hence the zero-energy wavefunction have no nodes, and we again identify it with the ground state wavefunction.

Turning back to the massless case, the absence of (positive energy) bound states can be loosely accounted for the Gauss curvature approaching zero as  $u$  approaches positive/negative infinity. This is because the effective potential stemming from the curvature of the surface is proportional to the Gauss curvature<sup>2</sup>. We therefore expect the potential barrier in the transformed one-dimensional problem,  $V_\ell(s)$ , to be roughly proportional to the Gauss curvature of the surface.

## VI. CONCLUSIONS AND OUTLOOK

We have studied the Dirac electrons on the helicoid so far. We saw that the scattering mainly occurs just around the helical axis and that the bound states are absent even when we make fermions massive.

One of the candidates of the physical realization of the present system is graphite with a screw dislocation. As our analysis was done using the Dirac equation and hence ignoring the actual lattice, the analysis is applicable when the typical length scale at which the carbon honeycomb lattice bends is much larger than the lattice constant.

Although we showed the absence of bound states of massless/massive Dirac electrons on the helicoid, we can also build surfaces that, unlike helicoid, allow bound states for massive/massless Dirac fermions. An example of such surfaces is the one whose metric is given by  $ds^2 = (dx^2 + dy^2)/(y^2 + A^2)$  with  $A$  being constant. This has a larger curvature at larger

distances and the corresponding effective potential is larger at greater distances.

Further extensions of our work may include applications to surfaces periodic in two or three directions rather than one. The Dirac equation on those surfaces can no longer be reduced to the ordinary Schrödinger-type equation unlike the case of the helicoid here.

We have considered only pseudo-spins in this paper. Thus another possible extension of the paper will be to introduce real spins into the analysis: this will be of great interest with more complicated spin-connections. This possible research direction is also thought-provoking as we might be able to consider spin current on graphene with combined pseudo- and real spins.

After the submission of the present work, we came to notice a paper which deals with helicoidal graphene nanoribbons<sup>10</sup>. While the screw axis region of helicoidal nanoribbons, which is the subject of the above paper, are hollow, our main interest in the present paper is the very region, because of its singularity and possible applications to graphite with a screw dislocation.

## VII. ACKNOWLEDGEMENT

The authors wish to thank Takahiro Morimoto for illuminating discussions at the early stages of the present study. The present work was supported by Grants-in-Aid for Scientific Research (Grant Nos. 25107005, 26247064) from MEXT and ImPACT from JST.

### Appendix A: Derivation of Eq. (26)

We take a notation in which  $x = s$  and  $k = E$  throughout this appendix. The one-dimensional Lippmann-Schwinger equation reads

$$\psi(x) = e^{ikx} - \frac{i}{2k} \int_{-\infty}^{\infty} dy e^{ik|x-y|} V(y) \psi(y). \quad (\text{A1})$$

Approximation à la Born gives the first-order perturbation:

$$\begin{aligned} \psi(x) &= e^{ikx} - \frac{i}{2k} \int_{-\infty}^{\infty} dy e^{ik|x-y|} V(y) e^{iky} \\ &= e^{ikx} - \frac{i}{2k} \left[ e^{-ikx} \int_x^{\infty} dy e^{2iky} V(y) + e^{ikx} \int_{-\infty}^x dy V(y) \right]. \end{aligned} \quad (\text{A2})$$

Hence the first-order perturbative expression for the transmission/reflection coefficients are

$$T = 1 - \frac{i}{2k} \int_{-\infty}^{\infty} dy V(y), \quad R = \frac{i}{2k} \int_{-\infty}^{\infty} dy e^{2iky} V(y). \quad (\text{A3})$$

We can readily see that  $T$  is invariant under space inversion<sup>17</sup> and that  $\arg T \sim 1/k$  for sufficiently large  $k$ . Similarly,

$$\begin{aligned} \int_{-\infty}^{\infty} dy e^{2iky} \frac{1}{1+y^2} &= \pi e^{-2|k|}, \\ \int_{-\infty}^{\infty} dy e^{2iky} \frac{y}{\sqrt{1+y^2}^3} &= 4ikK_0(2|k|) \sim 4ike^{-2|k|}. \end{aligned} \quad (\text{A4})$$

so that  $\arg R \sim 1/k$  for sufficiently large  $k$ . This completes the derivation of Eq. (26).

### Appendix B: Nonrelativistic Fermions on the Helicoid

We deal with the Schrödinger equation on the helicoid following the unpublished work by Aoki and Morimoto<sup>4</sup> cited in the introduction for the purpose of comparison with the Dirac case.

We first write down the Schrödinger equation on a curved surface with metric  $g_{ij}$ :

$$\left[ -\frac{\hbar^2}{2m} \frac{1}{\sqrt{g}} \frac{\partial}{\partial q^i} \sqrt{g} g^{ij} \frac{\partial}{\partial q^j} - \frac{\hbar^2}{8m} (\kappa_1 - \kappa_2)^2 \right] \phi(q^k) = E \phi(q^k), \quad (\text{B1})$$

where  $(q^1, q^2)$  is the coordinate system on the surface, denoted hereafter as  $(u, v)$ , and  $\kappa^1$  and  $\kappa^2$  are the two principal curvatures on the surface.

Specifically, the Schrödinger equation on the helicoid (metric given by (12)) becomes

$$\frac{1}{\cosh^2 u} \left( \frac{d^2}{du^2} + \ell^2 - \frac{1}{\cosh^2 u} \right) \phi(u) = E \phi(u). \quad (\text{B2})$$

We used the fact that the two principal curvatures of the helicoid is  $\kappa_{\pm} = \pm 1/(a \cosh^2(u))$ <sup>11</sup>. We also set  $a = 1$ ,  $\hbar = 1$  and  $m = 1/2$ , as in the case of the Dirac particles. Here, rather surprisingly, the coordinate transformation for the Dirac equation, Eq. (20) can also be applied to transform this Schrödinger equation into a new Schrödinger equation on the flat metric:

$$-\frac{d^2}{ds^2} \psi(s) + \left( \frac{\ell^2}{1+s^2} - \frac{s^2+2}{4(1+s^2)^2} \right) \psi(s) = E \psi(s). \quad (\text{B3})$$

The potential of this Schrödinger equation is  $V(s) = \frac{\ell^2}{1+s^2} - \frac{s^2+2}{4(1+s^2)^2}$ , which is different from that of the Dirac case.

We first note that the system does not allow for bound states, following a similar argument in the main body of the text. The absence of bound states on the helicoid, therefore, is just not specific to Dirac fermions.

We also see that the potential is symmetric with respect to  $\ell \mapsto -\ell$  and  $s \mapsto -s$ . This indicates that the reflection phase shift does not change by  $\pi$  at  $\ell = 0$ . This is one major difference in physical quantities between the Dirac and the Schrödinger case. As mentioned at the end of Section III C, the symmetry of the Dirac system is the combined inversion of the angular momentum and the (pseudo-)spin directions, whereas the allowed symmetry operation in the Schrödinger



case is to invert the angular momentum only – no spins are involved in the Schrödinger system.

LDoS of the Schrödinger system, shown in Fig. 11, behaves also differently from that of the Dirac system. The oscillation amplitude of LDoS does not diminish as we go farther away from the helical axis unlike the Dirac case.

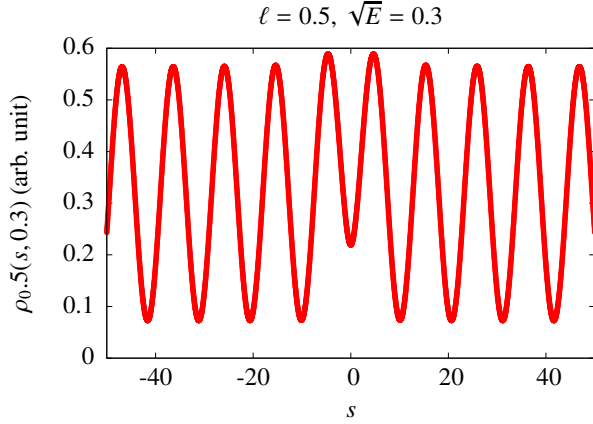


FIG. 11: (Color online) Local density of states in the Schrödinger case with  $\ell = 0.5$  at  $\sqrt{E} = 0.3$ .

\* Now at Kavli Institute for the Physics and Mathematics of the Universe, The University of Tokyo, Kashiwa, Chiba 277-8582, Japan ; Electronic address: masataka.watanabe@ipmu.jp

† Now at RIKEN Center for Emergent Matter Science (CEMS), Wako 351-0198, Japan

<sup>1</sup> H. Aoki and M. Dresselhaus, eds., *Physics of Graphene, NanoScience and Technology* (Springer, Heidelberg and New York, 2014), ISBN 9783319026336.

<sup>2</sup> H. Aoki, M. Koshino, D. Takeda, H. Morise, and K. Kuroki, *Phys. Rev. B* **65**, 035102 (2001), URL <http://dx.doi.org/10.1103/PhysRevB.65.035102>.

<sup>3</sup> O. Klein, *Zeitschrift für Physik* **53**, 157 (1929), ISSN 0044-3328, URL <http://dx.doi.org/10.1007/BF01339716>.

<sup>4</sup> H. Aoki and T. Morimoto, unpublished. The paper studied the electronic structure of the helicoid by using the Schrödinger equation.

<sup>5</sup> F. H. Horn, *Nature* (1952), URL <http://dx.doi.org/10.1038/170581a0>.

<sup>6</sup> J. Rakovan and J. A. Jaszczak, *American Mineralogist* **87**, 17 (2002).

<sup>7</sup> D. M. Bird and A. R. Preston, *Phys. Rev. Lett.* **61**, 2863 (1988), URL <http://dx.doi.org/10.1103/PhysRevLett.61.2863>.

<sup>8</sup> N. Birrell and P. Davies, *Quantum Fields in Curved Space*, Cambridge Monographs on Mathematical Physics (Cambridge University Press, 1984), ISBN 9780521278584.

<sup>9</sup> S.-S. Chern, *Proceedings of the American Mathematical Society* **6**, pp. 771 (1955), ISSN 00029939, URL <http://www.jstor.org/stable/2032933>.

<sup>10</sup> V. Atanasov and A. Saxena, *Phys. Rev. B* **92**, 035440 (2015), URL <http://link.aps.org/doi/10.1103/PhysRevB.92.035440>.

<sup>11</sup> A. Pressley, *Elementary Differential Geometry*, Springer Undergraduate Mathematics Series (Springer London, 2010), ISBN 9781848828919.

<sup>12</sup> The massive case with mass  $m$  are described by adding  $im\sigma^3\phi$  term to the left-hand side of the equation.

<sup>13</sup> Notice we have dropped 1/2 from the ordinary definition of  $\partial$  and  $\bar{\partial}$ .

<sup>14</sup> We can show this as follows:  $|A|^2 - |B|^2 = |C|^2 - |D|^2$  leads to  $|p|^2 - |q|^2 = |r|^2 - |s|^2 = 1$  and  $p^*r - q^*s = 0$ , which then leads to  $|p|^2 = |s|^2$ . This means there exists  $\Delta$  such that  $s = p^*e^{i\Delta}$  and substituting this into the relations above yields  $r = q^*e^{i\Delta}$ .

<sup>15</sup> Although we started off by dealing with *pseudo* spins on helical graphene, at this stage we are free to think of these spins as *real* spins; there would be no difference in any arguments in the paper according to whether spins are real or not.

<sup>16</sup> Change  $\ell$  into  $-\ell$  to see  $\psi_+(s)$  is also positive everywhere.

<sup>17</sup> That  $T$  is invariant under space inversion can also be seen by considering Wronskian and equating its values at  $x \rightarrow \pm\infty$ .